

# ADAPTIVELY WEIGHTED LEAST SQUARES FINITE ELEMENT METHODS FOR PARTIAL DIFFERENTIAL EQUATIONS WITH SINGULARITIES

B. HAYHURST\*, M. KELLER\*, C. RAI\*, X. SUN†, AND C. R. WESTPHAL\*‡

## Abstract.

The overall effectiveness of finite element methods may be limited by solutions that lack smoothness on a relatively small subset of the domain. In particular, standard least squares finite methods applied to problems with singular solutions may exhibit slow convergence, or in some cases, may fail to converge. By enhancing the norm used in the least squares functional with weight functions chosen according to a coarse-scale approximation, it is possible to recover near-optimal convergence rates without relying on exotic finite element spaces or specialized meshing strategies. In this paper we describe an adaptive algorithm where appropriate weight functions are generated from a coarse-scale approximate solution. Several numerical tests, both linear and nonlinear, illustrate the robustness of the adaptively weighted approach compared with the analogous standard  $L^2$  least squares finite element approach.

**Key words.** Adaptive Finite Element Methods, Weighted Norm Minimization, Singularities

**AMS subject classifications.** 65N30, 65N12, 35J20, 76D05

**1. Introduction.** In this paper we consider partial differential equations that exhibit singular behavior at isolated locations the domain. It is well known that problems with smooth data may fail to provide smooth solutions as a consequence of either the domain or the operator. To illustrate the main ideas, consider

$$\begin{cases} \mathcal{K}(u) = f & \text{in } \Omega \\ u = g & \text{on } \partial\Omega, \end{cases} \quad (1.1)$$

where  $\mathcal{K}$  is a second-order differential operator. If  $f \in L^2(\Omega)$  and  $g \in H^{3/2}(\Omega)$  is sufficient to guarantee that  $u \in H^2(\Omega)$ , then we consider the problem to have full regularity. We consider problems without this property to have a low regularity, or (potentially) nonsmooth solutions. For example, Poisson's equation is known to have full regularity when  $\Omega$  is convex, but can have nonsmooth solutions when  $\partial\Omega$  has corners (or edges) with interior angle greater than  $\pi$  [19]. This lack of smoothness is localized, however. In any subdomain excluding a neighborhood of each corner point the solution remains smooth. Other elliptic problems have similar behavior as a consequence of the domain, see e.g., [24, 25]. The operator  $\mathcal{K}$  can also induce a loss of smoothness when coefficients are either singular (i.e.,  $\rightarrow \infty$ ) or degenerate (i.e.,  $\rightarrow 0$ ) at distinct points in  $\Omega$  [5].

Invariably, numerical methods tend to suffer as a consequence of a loss of regularity. Finite element convergence rates can be reduced or, in some cases, the method can fail to converge to the solution of the problem. Moreover, in many situations, the loss of optimal rates of convergence is effective globally, even though the nonsmooth behavior of the solution is localized. This global effect from a local component is known as *the pollution effect*.

---

\*Department of Mathematics and Computer Science, Wabash College, Crawfordsville, IN 47933, email:{bzhayhur16, mgkeller17, csrai15, westphac}@wabash.edu.

†Department of Mathematics, University of Washington, Seattle, WA 98195-4350, email:sunx23@uw.edu.

‡This work was supported by the National Science Foundation under grant DMS-1216297.

A wide range of computational approaches have been developed to handle the difficulties induced by such singularities and encompass nearly all aspects of the overall numerical framework. In the finite element context, problems where singularities cause slow convergence can often be effectively treated with graded meshes or an adaptive mesh refinement strategy [30, 16, 1, 11]. In more extreme cases, where standard formulations would not yield discretization convergence, specialized finite element spaces can be employed to better match the low regularity inherent in the problem, for example, using Nédélec or Raviart-Thomas elements as in [6, 9].

In cases where the operator kernels are known analytically, an enhanced finite element basis can be constructed to capture singular solutions better than with standard polynomial bases [3, 4, 2, 35, 32]. Further, there are a number of paradigms that are designed around a weak variational formulation that seek solutions in lower order Sobolev spaces than more traditional approaches. In the context of discontinuous Galerkin (DG) and discontinuous Petrov-Galerkin (DPG) [17] methods, for example, continuity requirements in the trial and test spaces are relaxed and additional degrees of freedom on the element boundaries lead to additional jump conditions in the variational problem. Additionally, in the least squares finite element context, for example, dual space norms induced by the operator adjoint can replace standard  $L^2$  norms to relax regularity requirements [8, 13]. The methodology we propose here has parallels to each of these ideas.

In this work we introduce an adaptively weighted least squares finite element approach for problems with singularities. By generalizing the standard least squares functional with weighted norms, we may essentially redistribute the strength by which the variational problem is enforced across the domain. The use of weighted norms and weighted inner products is, of course, not a new idea. Using weighted norms to generalize  $L^2$  residual minimization problems allows for robust treatment of problems with boundary singularities in weighted  $H^1(\Omega)$  or  $H(\text{div})$  norms [27, 28, 14]. Though this approach is effective, it requires the explicit construction of a weight function localized to each singular point in the domain. Here we use a sequence of coarse-scale approximations to generate a customized weighted norm in which to minimize the error. This adaptive approach can reproduce the effectiveness of the weighted norm least squares approach, but with the advantage of not requiring the *a priori* knowledge of either the power or location of any singularity. By analogy, this is similar to the advantage of adaptive mesh refinement in allowing approximate solutions to guide the construction of an optimal mesh. In [34], this adaptive approach is used in a weighted Galerkin formulation for problems with boundary layers.

The organization of this paper is as follows. In the next section, we formally introduce the idea of a weighted least squares finite element method. In section 3 we provide details of an adaptive framework for choosing effective weight functions from a sequence of coarse scale approximations. In section 4 we provide several numerical examples that illustrate the robustness of the method.

**2. Notation and Background.** Throughout this paper,  $\Omega$  and  $\partial\Omega$  represent the domain and boundary of the PDE, which has a non-smooth solution at distinct locations in  $\bar{\Omega}$ . We use standard notation for the  $L^2(\Omega)^d$  norm,  $\|\cdot\|$ , and inner product,  $\langle \cdot, \cdot \rangle$ , and use  $\|\cdot\|_D$  to denote the  $L^2$  norm on subdomain  $D \subseteq \Omega$ .

We consider the least squares finite element approach to problems of the form in (1.1). Let  $LU = F$  be a linear, first-order reformulation of (1.1). For nonlinear problems,  $L$  represents a linearization about a current approximation and the solution procedure would involve a sequence of such linearized problems. In either case, we

thus require finding a finite element approximation to  $U$  in the function space  $\mathcal{V}$ . The standard  $L^2$  least squares method here is to define the least squares functional,

$$\mathcal{F}(U; F) = \|LU - F\|^2, \quad (2.1)$$

and minimize over  $\mathcal{V}$ : find  $U \in \mathcal{V}$  such that  $\mathcal{F}(U; f) \leq \mathcal{F}(V; f) \quad \forall V \in \mathcal{V}$ . This minimization problem is equivalent to the variational problem: find  $U \in \mathcal{V}$  such that

$$\langle LU, LV \rangle = \langle F, LV \rangle \quad \forall V \in \mathcal{V}.$$

In general, we assume a least squares finite element formulation that is well-posed and robust for smooth-problems. In many cases these formulations contain additional consistent constraints. The weighting procedure here is designed to extend such a formulation to recover optimal (or nearly optimal) behavior in the presence of nonsmooth solutions.

For the general weighted least squares method, let  $w : \bar{\Omega} \rightarrow [0, 1]$  denote a weight function (possibly different for each equation), and define the weighted least squares functional,

$$\mathcal{F}_w(U; F) = \|w(LU - F)\|^2. \quad (2.2)$$

Similar to the standard approach, minimizing  $\mathcal{F}_w$  over  $U \in \mathcal{V}$  is equivalent to finding  $U \in \mathcal{V}$  such that

$$\langle wLU, wLV \rangle = \langle wF, wLV \rangle \quad \forall V \in \mathcal{V}.$$

The weighted least squares approach has been used effectively for problems with singular behavior, essentially seeking to recover optimal finite element convergence rates away from the singular points and rates similar to the interpolant near singularities. In [27, 28, 14] the weighted least squares approach is developed using weight functions based on the asymptotic behavior of the solutions near singularities. In [5] a similar approach is taken for a problem with singular/degenerate coefficients. Adopting this idea in practice has been used effectively for other applications (e.g., for incompressible fluids [29, 15]) and provides a flexible and straightforward way to modify a least squares finite element method in the presence of singularities. This approach requires *a priori* knowledge of the location and an estimate of the asymptotic behavior of each point of nonsmoothness to define an appropriate weight function. In the following section, we develop a general adaptive approach that does not require this *a priori* information, but rather builds an optimal composite weight function based on a coarse scale approximate solution that requires no explicit user input.

**3. The Adaptively Weighted Least Squares Approach.** Let  $\Omega^h$  represent a triangulation of the domain and  $\mathcal{V}^h$  an associated finite element space in which we will approximate the solution. Given a weight function  $w$ , the discrete solution  $U^h$  is the unique minimizer of  $\mathcal{F}_w(U^h; F)$  over  $\mathcal{V}^h$ : find  $U^h \in \mathcal{V}^h$  such that

$$\mathcal{F}_w(U^h; F) \leq \mathcal{F}_w(V^h; F) \quad \forall V^h \in \mathcal{V}^h. \quad (3.1)$$

The adaptive approach is based on defining  $w$  from a current approximation to the exact solution. For this, we define an element-wise measure of the approximation gradient,

$$\mathcal{G}(\tau) = \frac{1}{\mu(\tau)} \|\nabla U^h\|_{\tau}, \quad (3.2)$$

where  $\mathcal{G}_i = \mathcal{G}(\tau_i)$  is the value on  $\tau_i$ , the  $i^{\text{th}}$  element of  $\Omega^h$ . In cases where the elements are of vastly different scales we take  $\mu(\tau) = h_\tau^2$  as a measure of the area of the element, making  $\mathcal{G}(\tau)$  a measure of error density. With quasiuniform meshes,  $\mu(\tau) = 1$  can be used. We now define  $\mathcal{G}$  as a piecewise constant function on  $\Omega^h$ . The maximum and minimum values of  $\mathcal{G}$  are denoted by

$$\mathcal{G}_{min} = \min_{\tau_i \in \Omega^h} \mathcal{G}_i \quad \text{and} \quad \mathcal{G}_{max} = \max_{\tau_i \in \Omega^h} \mathcal{G}_i.$$

Locations with large/small gradients imply that the weight function should be chosen small/large (see e.g., [27, 28, 14]). By redefining the metric under which the error is minimized in this way, the variational problem is weakened in regions where the solution is most difficult to approximate.

We give two options for constructing  $w$  as a piecewise constant function from  $\mathcal{G}$ :

$$w_i = \frac{\mathcal{G}_{max} - \mathcal{G}_i}{\mathcal{G}_{max} - \mathcal{G}_{min}} + \frac{\mathcal{G}_{min}}{\mathcal{G}_{max}}. \quad (3.3)$$

or

$$w_i = \frac{c}{\mathcal{G}_i + c}, \quad \text{where} \quad c = \frac{\mathcal{G}_{min}\mathcal{G}_{max}}{\mathcal{G}_{max} - \mathcal{G}_{min}}, \quad (3.4)$$

In each, (3.3) and (3.4),  $w_i \leq 1$  and  $w_i = w_{min} = \mathcal{G}_{min}/\mathcal{G}_{max}$  when  $\mathcal{G}_i = \mathcal{G}_{max}$ . Figure 3.1 illustrates the shape function for each case (affine and inverse) and suggests a range of other empirical options.

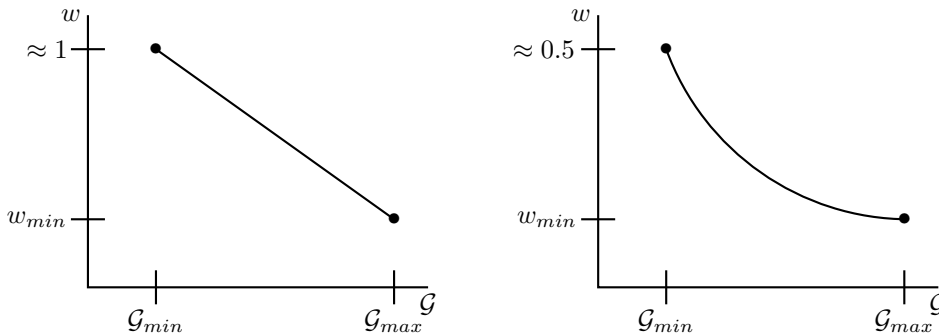


FIG. 3.1. Two shape function options for constructing the weight function. The affine model (left) reflects equation (3.3) and the inverse model (right) illustrates (3.4).

In an iterative framework, the basic adaptively weighted least squares method is described in algorithm 1.

The framework here is quite flexible and may be thought of analogously to the idea of adaptive mesh refinement, where a sequence of increasingly accurate approximations is found by successively redefining the weight function and resolving a finer scale and higher resolution problem. The mesh refinement step allows the weight function to be developed through coarse scale approximations which are relatively computationally inexpensive. Stopping criteria for the algorithm can be based on a single metric, like the global value of the least squares functional (2.2), or by the total number of refinement levels desired. For nonlinear problems, an indicator of how well the nonlinear error is resolved can involve a measure of the change between

---

**Algorithm 1** Adaptively Weighted Least Squares Framework.
 

---

**Start:** Initially set  $w = 1$  uniformly; choose initial mesh  $\Omega^h$

**Solve:** Obtain initial solution  $U_{old}^h$  by solving (3.1)

**while** ( overall accuracy < goal ) {

**Refine Mesh:** (Optional) Uniformly or adaptively

**while** ( nonlinear error estimate > tolerance ) {

**Re-Linearize:** about  $U_{old}^h$  (for nonlinear problems)

**Construct Weight:** Use  $U_{old}^h$  to define  $G_i$  from (3.2) and  $w_i$  from (3.3) or (3.4)

**Re-solve:** Using  $w$ , find  $U^h$  by solving (3.1); set  $U_{old}^h \leftarrow U^h$

  }

}

}

---

iterates or a comparison between a linear and nonlinear functional. It is also possible to simply take a fixed number of linearization steps on each mesh level, refining the weight function at each opportunity.

In [27, 28, 14], several weighted norm least squares methods are designed around minimizing the approximation error in weighted Sobolev spaces, where the weight functions are chosen according to the asymptotic nature of the solution. For example, in [27], assume  $U \sim r^{\alpha-1}$  represents the asymptotic behavior of the solution to  $LU = F$  near a boundary singularity, where  $r$  is the distance to the singular point and  $\alpha \in (0, 1)$  represents the power of the singular solution. A simple calculation indicates that  $U \in H^s(\Omega)$  for  $s < \alpha \in (0, 1)$ . The *a priori* weight function described in [27] requires choosing  $w \sim r^\beta$  such that  $wU \in H^2(\Omega)$ , which indicates  $\beta \gtrsim 2 - \alpha$ . With a weight function of this design, it is proved that optimal finite element error convergence in a weighted Sobolev space is expected. This indicates that the pollution effect is eliminated, yielding the same convergence as the  $L^2$  interpolant in a neighborhood of the singular point and optimal convergence in a neighborhood excluding the singularity. For the adaptive approach, we mimic this by choosing the weight construction in (3.4), where we see that asymptotically

$$w \sim \frac{1}{|\nabla U|} \sim r^{2-\alpha},$$

which matches the *a priori* construction described in [27]. Analysis of the weighted least squares methods in [27, 28, 14] is done in the context of a hierarchy of Sobolev spaces weighted by powers of  $r$ , whereas here we have a set of spaces weighted by an evolving approximate solution.

In the following section we present several numerical tests that illustrate the utility of the adaptively weighted approach described here. The first two examples have a known analytic solution and the convergence, both near the singularity and away from it, is carefully monitored to show how the adaptive approach improves convergence. The remaining examples provide a variety of other measures to illustrate the effectiveness and flexibility of the adaptive approach.

**4. Numerical Results.** In this section we provide several numerical examples to illustrate the effectiveness and robustness of the adaptively weighted least squares approach as described in algorithm 1. In the first example, we consider a div/curl first

order system induced by the Laplace operator. In this context, regularity dictates that the standard least squares approach using  $H^1$  conforming elements is not applicable for non-convex domains. Weighted least squares methods can be used to recover optimal convergence in a weighted  $H^1$  norm (see, e.g., [27, 28]), and the results here show that the adaptively weighted approach achieves similar results, but does so with no explicit *a priori* information provided by the user. The second example applies the adaptively weighted approach to a singularly perturbed elliptic operator that induces a nonsmooth solution at an interior point in the domain. Here, a mixed least squares finite element formulation is examined and the adaptively weighted approach increases slow convergence induced by the loss of smoothness in the solution. In the next example, we consider a div/curl least squares formulation of the incompressible Stokes' equations in a non-convex domain. We show how the adaptively weighted approach ameliorates the pollution effect, yields optimal convergence in the weighted least squares functional norm, and gives asymptotically accurate approximations to the velocity in the neighborhood of a reentrant corner. In addition we show that the adaptively weighted approach improves mass conservation in the example. The next two examples illustrate the algorithm in the framework of a nonlinear problem. In these cases we consider two different formulations of the stationary Navier-Stokes equations applied to standard benchmark problems (the lid-driven cavity and flow over a square obstacle).

All computational results are implemented in FreeFem++ [21].

**4.1. Example 1: Poisson on the L-Shaped Domain.** For this example we define  $\Omega = \{(x, y) \in (-1, 1)^2 : (x, y) \notin [0, 1) \times (-1, 0]\}$ , the L-shaped domain pictured in figure 4.1. We also define a partition of the domain to distinguish between a neighborhood of the singular point and the rest of the domain:  $\Omega_0 = \{(x, y) \in \Omega : x^2 + y^2 < (0.25)^2\}$  denotes the neighborhood of the origin and  $\Omega_1 = \Omega \setminus \Omega_0$  represents the remainder of the domain in which the solution is smooth.

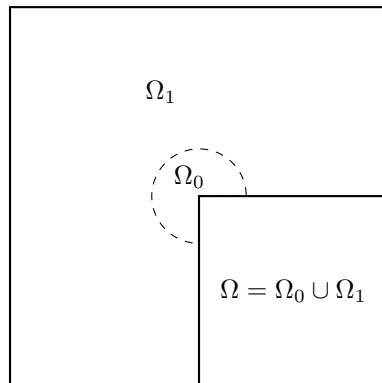


FIG. 4.1. L-shaped domain for Numerical Example 1:  $\Omega$  is partitioned into subdomains  $\Omega_0$  and  $\Omega_1$  to distinguish global convergence from local convergence near the singular point.

We consider numerically approximating a nonsmooth solution to the problem

$$\begin{cases} \Delta p = f & \text{in } \Omega, \\ p = p^* & \text{on } \partial\Omega, \end{cases} \quad (4.1)$$

where we take  $f = 0$ , and the boundary data is chosen so that the exact solution corresponds to  $p^* = r^{2/3} \sin(2\theta/3)$  and  $(r, \theta)$  corresponds to a local polar coordinate

system centered at the origin. The exact solution here is in the kernel of the Laplacian and represents the nonsmooth component of a typical Poisson problem on a domain with a reentrant corner of interior angle  $3\pi/2$ .

We introduce the flux variable  $\mathbf{u} = \nabla p$  and consider the expanded first-order system,

$$\begin{cases} \nabla \cdot \mathbf{u} = f & \text{in } \Omega, \\ \nabla \times \mathbf{u} = 0 & \text{in } \Omega, \\ \mathbf{u} - \nabla p = \mathbf{0} & \text{in } \Omega, \\ \hat{\boldsymbol{\tau}} \cdot \mathbf{u} = \hat{\boldsymbol{\tau}} \cdot \nabla p^* & \text{on } \partial\Omega, \\ p = p^* & \text{on } \partial\Omega, \end{cases} \quad (4.2)$$

where  $\hat{\boldsymbol{\tau}}$  is the counterclockwise unit tangent vector to  $\partial\Omega$ . The boundary condition on  $\mathbf{u}$  is found by differentiating the boundary data on  $p^*$ , and though this equation is redundant, including it generally improves the quality of approximations on coarse meshes. In this example, boundary conditions on  $\mathbf{u}$  and  $p$  are imposed strongly, though there are a range of boundary condition treatments possible in the least squares context. The associated weighted least squares functional is

$$\mathcal{F}_w(\mathbf{u}, p; f) = \|w(\nabla \cdot \mathbf{u} - f)\|^2 + \|w\nabla \times \mathbf{u}\|^2 + \|w(\mathbf{u} - \nabla p)\|^2, \quad (4.3)$$

which we minimize over standard continuous P1 elements for each unknown, enforcing boundary conditions on  $p$  and  $\mathbf{u}$  strongly. We follow algorithm 1 for the iterative approach, and for this problem (3.2) takes the form

$$\mathcal{G}(\tau) = (\|\nabla p^h\|_\tau^2 + \|\nabla \mathbf{u}^h\|_\tau^2)^{1/2}$$

on each element  $\tau_i$ . The piecewise constant weight function in each step is computed according to (3.4).

In Table 4.1 convergence is summarized for the adaptively weighted approach as well as the standard approach (corresponding to  $w = 1$ ). Since the exact solution is known, we report the  $L^2$  error in both  $p$  and  $\mathbf{u}$  and in both  $\Omega_0$  and  $\Omega_1$ . In each case, a quasi-uniform mesh is used with  $N$  total elements, and for the adaptive approach we take three iterations on each mesh and report the values at the third iteration.

A simple calculation reveals that  $p^* \in H^{1+s}(\Omega)$  and  $\mathbf{u}^* = \nabla p^* \in H^s(\Omega)^2$  for  $s < 2/3$ . Since  $\mathbf{u}^* \notin H^1(\Omega)$ , convergence is not guaranteed for the standard LS approach, and it fails as expected. The adaptive approach performs better, showing near optimal convergence rates for the  $L^2$  error for both  $p$  and  $\mathbf{u}$  in each subdomain. The least squares functional norm, which is essentially a weighted  $H^1$  seminorm, converges at the optimal rate. This shows that we can retain the convenience of using  $H^1$  conforming finite element spaces, even when regularity indicates that the solution is not in  $H^1(\Omega)$  locally.

Standard LS ( $w = 1$ )

$N$	$\mathcal{F}^{1/2}$	$\ p^* - p^h\ _{\Omega_0}$	$\ p^* - p^h\ _{\Omega_1}$	$\ \mathbf{u}^* - \mathbf{u}^h\ _{\Omega_0}$	$\ \mathbf{u}^* - \mathbf{u}^h\ _{\Omega_1}$
1716	1.22	0.0166	0.0454	0.389	0.448
6898	1.21	0.0157	0.0439	0.382	0.439
27742	1.20	0.0152	0.0431	0.377	0.434
rate $\approx$	0	0	0	0	0

Adaptively Weighted LS

$N$	$\mathcal{F}_w^{1/2}$	$\ p^* - p^h\ _{\Omega_0}$	$\ p^* - p^h\ _{\Omega_1}$	$\ \mathbf{u}^* - \mathbf{u}^h\ _{\Omega_0}$	$\ \mathbf{u}^* - \mathbf{u}^h\ _{\Omega_1}$
1716	0.136	0.00140	0.000595	0.1427	0.0470
6898	0.0755	0.000313	0.000132	0.0855	0.0151
27742	0.0407	0.000104	0.0000412	0.0524	0.00441
rate $\approx$	0.89	1.58	1.68	0.71	1.78
optimal rate	1	1.66	2	0.66	2

TABLE 4.1

Convergence comparison between the standard least squares approximation ( $w = 1$ ) and the adaptively weighted approach. Convergence rate is estimated from results on the two finest levels and the optimal rate is based on standard interpolation bounds for the exact solution.

To illustrate the character of the weight function generated by this approach, figure 4.2 shows the weight generated on the coarsest mesh for the results in table 4.1. Smaller values of  $w$  (in darker color) occur near the reentrant corner. For context, the example in table 4.1 produces weight with  $\|w^h\|_{L^2(\Omega)} \approx 0.876$ , which in absolute magnitude does not substantially differ from the scale under uniform weighting, which gives  $\|1\|_{L^2(\Omega)} = \sqrt{3} \approx 1.73$  for this example.

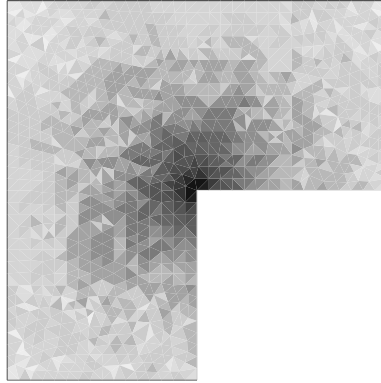


FIG. 4.2. Adaptively generated weight function for domain with  $N = 1716$  elements. Larger values are lighter ( $w_{max} = 0.507$ ); smaller values are darker ( $w_{min} = 0.0281$ ).

In this example the domain had one singular point, but applying the method to a problem with multiple singularities is analogous and straightforward.

**4.2. Example 2: A Singularly Perturbed Elliptic Problem.** For this example we treat a problem with a singularity in the interior of the domain, induced by the operator rather than the geometry of the boundary. Consider the following

problem:

$$\begin{cases} -\nabla \cdot (r^{2\beta} \nabla u) + r^{2\alpha} u = f & \text{in } \Omega, \\ u = 0 & \text{on } \partial\Omega, \end{cases} \quad (4.4)$$

where  $\Omega = (-1, 1)^2$  and  $r$  is the coordinate distance from  $(0, 0)$ . When the coefficients are degenerate (i.e., go to zero) or singular (i.e., blow up) at an interior point, as is possible here, the solution may be non-smooth in a neighborhood of the origin. In [5], a weighted-norm least squares finite element method is developed for (4.4) where the weight function is chosen by the expected regularity of the problem. For this example, we choose  $\beta = 0.5$  and  $\alpha = -0.5$ , which induces a solution with asymptotic behavior of  $r^\lambda$  for  $\lambda \approx 0.618034$ . The function  $f$  is chosen so that the exact solution is given by

$$u = (1 - x^2)(1 - y^2)r^\lambda,$$

which exhibits the expected nonsmooth behavior at the origin, but satisfies homogeneous Dirichlet boundary conditions. For this example we recall the weighted least squares approach in [5], but apply the adaptive approach in choosing the weight function.

Let  $\boldsymbol{\sigma} = -r^{2\beta} \nabla u$  and define the weighted least squares functional

$$\mathcal{F}_w(u, \boldsymbol{\sigma}; f) = \|w(\nabla \cdot \boldsymbol{\sigma} + r^{2\alpha} u - f)\|^2 + \|w(\boldsymbol{\sigma} + r^{2\beta} \nabla u)\|^2.$$

We use a uniform triangulation of  $\Omega$  and approximate  $\boldsymbol{\sigma}$  in the lowest order  $H(\text{div})$  conforming Raviart-Thomas finite element space, RT0, and use conforming P1 elements for  $u$ , with boundary conditions on  $u$  enforced strongly. As in example 1, we define a partition of  $\Omega$ , where  $\Omega_0 = (-0.2, 0.2)^2$  represents a fixed neighborhood of the origin and  $\Omega_1 = \Omega \setminus \Omega_0$  is the remainder of the domain.

We follow algorithm 1 for the iterative approach, and use

$$\mathcal{G}(\tau) = (\|\nabla u\|_\tau^2 + \|\nabla \boldsymbol{\sigma}\|_\tau^2)^{1/2}$$

as the element-wise gradient measure and use (3.4) for the construction of  $w$  from  $\mathcal{G}$ . Table 4.2 summarizes numerical results on four nested mesh levels. The standard least squares approach shows results typical of a problem with reduced regularity. Even though the functional norm decreases at approximately  $\mathcal{O}(h)$ , the  $L^2$  error of  $u$  shows slow convergence, even in the subdomain away from the origin. The adaptively weighted approach yields similarly slowly decreasing errors near the origin, but faster convergence in the rest of the domain.

$N$	Standard LS ( $w = 1$ )			Adaptively Weighted LS		
	$\mathcal{F}^{1/2}$	$\ u - u^h\ _{\Omega_0}$	$\ u - u^h\ _{\Omega_1}$	$\mathcal{F}_w^{1/2}$	$\ u - u^h\ _{\Omega_0}$	$\ u - u^h\ _{\Omega_1}$
512	0.591	0.0154	0.0133	0.591	0.0154	0.0133
2048	0.299	0.00817	0.00270	0.0707	0.00668	0.00704
8192	0.150	0.00406	0.00151	0.0336	0.00314	0.00175
32768	0.0756	0.00222	0.000874	0.0148	0.00183	0.000512
rate $\approx$	0.99	0.87	0.79	1.18	0.78	1.77

TABLE 4.2

Numerical results for example 3. Convergence rates are computed relative to the two finest mesh levels.

For the formulation used for this problem, it's important to recognize the challenge here is somewhat different from the previous examples. In example 1, the flux variable fails to be in  $H^1(\Omega)$  in a neighborhood of the corner point, but we still use a finite element subspace of  $H^1$  for its approximation. Thus, the standard approach cannot be expected to converge. Here we have  $u \in H^1(\Omega)$  and  $\boldsymbol{\sigma} \in H(\text{div}) = \{\mathbf{v} \in L^2(\Omega)^2 : \nabla \cdot \mathbf{v} \in L^2(\Omega)\}$ , which is consistent with the approximating spaces, though not smooth enough to achieve optimal  $L^2$  rates. The standard approach converges, albeit slowly, and the adaptively weighted approach serves to weaken the problem enough near the origin to enhance the convergence away from the origin, i.e., mitigating the pollution effect.

**4.3. Example 3: Stokes Flow.** For this example we consider steady incompressible flow in  $\Omega \subset \mathbb{R}^2$  modeled by Stokes' equations,

$$\begin{cases} -\Delta \mathbf{u} + \nabla p = 0 & \text{in } \Omega, \\ \nabla \cdot \mathbf{u} = 0 & \text{in } \Omega, \\ \mathbf{u} = \mathbf{g} & \text{on } \partial\Omega, \end{cases} \quad (4.5)$$

where  $\mathbf{u} = (u_1, u_2)$  represents fluid velocity,  $p$  is the pressure, and  $\mathbf{g}$  gives the velocity on the boundary,  $\partial\Omega$ . By introducing the velocity gradient  $\mathbf{U} = \nabla \mathbf{u}$ , system (4.5) can be reformulated to the first order system

$$\begin{cases} -\nabla \cdot \mathbf{U} + \nabla p = \mathbf{0} & \text{in } \Omega, \\ \nabla \times \mathbf{U} = \mathbf{0} & \text{in } \Omega, \\ \mathbf{U} - \nabla \mathbf{u} = \mathbf{0} & \text{in } \Omega, \\ \nabla \cdot \mathbf{u} = 0 & \text{in } \Omega, \\ \mathbf{u} = \mathbf{g} & \text{on } \partial\Omega, \\ \hat{\boldsymbol{\tau}} \cdot \mathbf{U} = \hat{\boldsymbol{\tau}} \cdot \nabla \mathbf{g} & \text{on } \partial\Omega, \end{cases} \quad (4.6)$$

where  $\hat{\boldsymbol{\tau}}$  is a unit tangent vector to  $\partial\Omega$ . Including the curl constraint of  $\mathbf{U}$  into the system is an additional, yet consistent, constraint from the definition of  $\mathbf{U}$ . Additionally we note that  $U_{11} + U_{22} = \nabla \cdot \mathbf{u} = 0$ , and we directly substitute  $U_{22} = -U_{11}$  to (4.6), reducing the total unknowns by one.

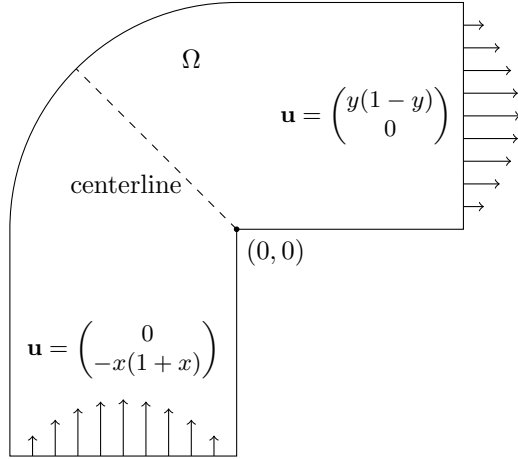


FIG. 4.3. Stokes flow domain and boundary conditions. Inflow and outflow boundary values are shown; no-slip conditions apply to other walls. Conservation of mass is measured as the velocity flux across the diagonal line along  $y = -x$ .

The standard div/curl least squares approach is to minimize the functional

$$\mathcal{F}(\mathbf{u}, \mathbf{U}, p) = \|\nabla \cdot \mathbf{U} - \nabla p\|^2 + \|\nabla \times \mathbf{U}\|^2 + \|\mathbf{U} - \nabla \mathbf{u}\|^2 + \|\nabla \cdot \mathbf{u}\|^2$$

over an appropriate space of functions for each unknown. When  $\Omega$  is sufficiently smooth and convex, the norm induced by  $\mathcal{F}$  is equivalent to the  $H^1(\Omega)$  norm of each unknown (up to a constant for  $p$ ) and accurate discrete approximations can be found using standard conforming piecewise polynomial spaces for each unknown. For nonconvex domains,  $\mathbf{U}$  cannot be guaranteed to remain in  $H^1(\Omega)$  and the  $H^1$  equivalence of LS functional norm breaks down. This well-known loss of regularity has severe consequences for the standard div/curl LS approach – similar to examples 1 and 2, singularities at non convex corners can cause a loss of convergence and inaccurate solutions globally. System (4.6) is certainly not the only first-order formulation of (4.5), and the literature in least squares finite elements reflects a wide range of choices with different advantages and disadvantages (see e.g., [20, 22, 12]). The div/curl approach does not require exotic finite element spaces, it admits realistic boundary conditions for  $\mathbf{U}$ , and it tends to yield linear systems that can be solved robustly by multigrid methods. However, this system exhibits a loss of regularity (see e.g., [23, 10, 26]), which is what makes the weighted norm approach a compelling way to deal with problems with singularities.

For the adaptively weighted least squares approach, we directly follow the procedure defined in algorithm 1, defining the weighted least squares functional by

$$\mathcal{F}_w(\mathbf{u}, \mathbf{U}, p) = \|w(\nabla \cdot \mathbf{U} - \nabla p)\|^2 + \|w\nabla \times \mathbf{U}\|^2 + \|w(\mathbf{U} - \nabla \mathbf{u})\|^2 + \|w\nabla \cdot \mathbf{u}\|^2,$$

where  $w$  is chosen from a previous approximation according to element-wise values of

$$\mathcal{G}(\tau) = \|\nabla \mathbf{u}^h\|_\tau^2 + \|\nabla \mathbf{U}^h\|_\tau^2 + \|\nabla p^h\|_\tau^2,$$

and  $w$  is constructed according to (3.4). All unknowns are approximated with continuous P2 elements. We follow the nested iteration approach, where the initial approximation is computed on a coarse quasi-uniform mesh, a weight function is generated

on this mesh, (see figure 4.3), then the mesh is refined uniformly by splitting each element into four elements, and the next iterate is computed on the refined mesh. This is then repeated for a total of four refinement levels.

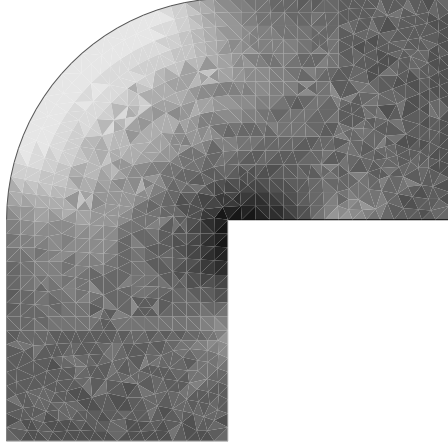


FIG. 4.4. *Adaptively generated weight function for Stokes flow example problem . Shown in greyscale is the first adaptive weight function, based on the initial approximation on mesh with  $h^{-1} = 16$ . (Larger values are lighter; smaller values are darker.)*

Since no exact solution is available for this problem we consider several metrics of convergence. First is the least squares functional norm,  $\mathcal{F}_w(\mathbf{u}^h, \mathbf{U}^h, p^h)^{1/2}$ , which includes the weight function used in finding the approximate solution. The second metric we use is the unweighted residual norm evaluated on a subdomain that excludes a neighborhood of the singularity:

$$\mathcal{R}^{1/2} = (\|\nabla \cdot \mathbf{U}^h - \nabla p^h\|_{\Omega_1}^2 + \|\nabla \times \mathbf{U}^h\|_{\Omega_1}^2 + \|\mathbf{U}^h - \nabla \mathbf{u}^h\|_{\Omega_1}^2 + \|\nabla \cdot \mathbf{u}^h\|_{\Omega_1}^2)^{1/2},$$

where  $\Omega_1 = \{(r, \theta) \in \Omega : r > 0.1\}$ . Figure 4.5 shows convergence results a comparison of convergence between the standard least squares approach with the adaptively weighted approach. As in examples 1 and 2, the standard approach stalls, while the adaptive approach converges at nearly optimal rates. Strong convergence in both the functional and residual norms shows that no significant pollution effect is present in the weighted norm approximations.

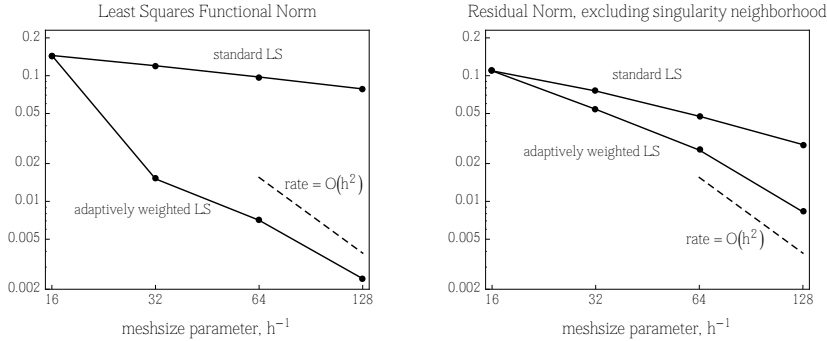


FIG. 4.5. Convergence comparison between standard least squares solution vs. adaptively weighted approach for increasing refinement level. The left shows the least squares functional norm,  $\mathcal{F}^{1/2}$ , for the standard approach and the weighted functional norm,  $\mathcal{F}_w^{1/2}$ . The right shows the  $L^2$  residual norm in a subdomain excluding a neighborhood of the singularity.

To examine the quality of the solution near the singularity we consider the velocity approximates near the reentrant corner. Through asymptotic analysis, it can be shown that  $\mathbf{u} \sim r^{0.544}$  near the origin for this problem. Figure 4.6 gives a log-log plot of the trace of  $u_1$  along the line  $y = -x$  in  $\Omega$ , which matches the asymptotic rate well, giving confidence that the method is reproducing a locally accurate solution.

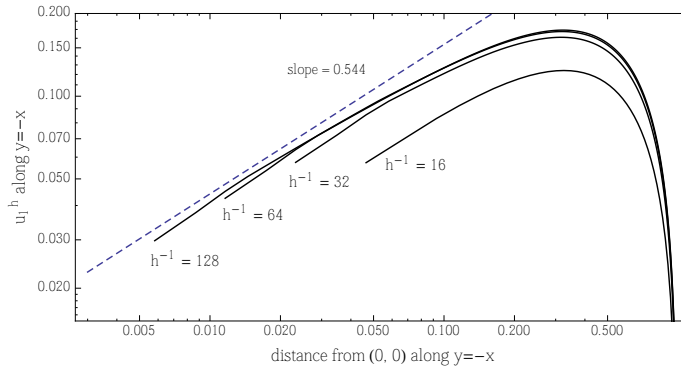


FIG. 4.6. Trace of  $u_1^h$  along the line  $y = -x$  through  $\Omega$  for increasing refinement level. The log-log scale shows the asymptotic behavior  $u_1^h \sim r^{0.544}$ .

As a final consideration, we measure the mass flux along the centerline of the domain (see figure 4.3) relative to the inflow. Least squares finite element methods typically enforce conservation of mass by minimizing the least squares functional which includes  $\nabla \cdot \mathbf{u} = 0$  as one term. Thus, the error in this term is balanced with the other equations in the system, giving conservation of mass errors on the order of the total discretization error. Rebalancing terms in the functional can improve approximation accuracy in one term at the expense of the others, and it is common to rescale the mass term by a large constant to reduce mass loss. We note that this should be done with caution, since introducing a large constant will result in lower accuracy in other terms and can degrade the conditioning of the resulting linear system drastically. In table 4.3 we show the relative mass loss in the adaptively weighted approach vs. the standard least squares approach, showing a significant improvement and further evidence that

the weighted approach eliminates pollution effects induced by the singularity at the corner.

% of mass loss at center line		
$h^{-1}$	Adaptive	Standard LS
16	30.6%	30.6%
32	7.04%	21.3%
64	2.05%	14.2%
128	0.694%	9.17%

TABLE 4.3

Mass loss at center line of symmetry for the adaptively weighted approach versus the standard approach. Both approaches used the same sequence of triangulations of  $\Omega$  with meshsize parameter  $h$ .

**4.4. Example 4: Navier-Stokes, Lid-Driven Cavity.** Here we consider the following div/curl formulation of steady incompressible flow in  $\Omega \subset \mathbb{R}^2$  as modeled by the first-order system

$$\left\{ \begin{array}{ll} -\nabla \cdot \mathbf{U} + Re\mathbf{U}\mathbf{u} + \nabla p = \mathbf{0} & \text{in } \Omega, \\ \mathbf{U} - \nabla \mathbf{u} = \mathbf{0} & \text{in } \Omega, \\ \nabla \cdot \mathbf{u} = 0 & \text{in } \Omega, \\ \nabla \times \mathbf{U} = 0 & \text{in } \Omega, \\ \nabla(\text{tr}(\mathbf{U})) = \mathbf{0} & \text{in } \Omega, \\ \mathbf{u} = \mathbf{g} & \text{on } \partial\Omega, \\ \hat{\boldsymbol{\tau}} \cdot \mathbf{U} = \hat{\boldsymbol{\tau}} \cdot \nabla g & \text{on } \partial\Omega, \end{array} \right. \quad (4.7)$$

where  $\text{tr}(\mathbf{U})$  is the trace of  $\mathbf{U}$ ,  $\hat{\boldsymbol{\tau}}$  is a unit tangent vector to  $\partial\Omega$ , and  $Re$  is the dimensionless Reynolds number, defined to be the ratio of inertial forces to viscous forces. At low  $Re$ , flow is essentially laminar; as  $Re$  increases, flow becomes more turbulent. The nonlinearity induced by the  $Re\mathbf{U}\mathbf{u}$  term makes (4.7) a natural candidate for the adaptive weighting procedure since iteration will already be necessary to resolve the nonlinearity. We present results for Stokes flow ( $Re = 0$ ) and turbulent flow at  $Re = 100$  in the lid-driven cavity (LDC) domain shown in figure 4.7

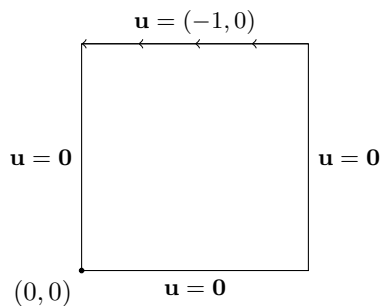


FIG. 4.7. Domain and boundary conditions for the lid-driven cavity test problem.

Despite the nonphysical nature of the problem, lid-driven cavity flow remains a well-studied standard test problem for fluid dynamics codes. Our standard for accuracy is the data presented in [18].

The discontinuous boundary conditions on  $\mathbf{u}$  in LDC flow induce strong singularities in  $p$  and in some components of  $\mathbf{U}$  which exclude them from  $L^2(\Omega)$  in the neighborhood of the two upper corners (see [7] for details). This poses a different, seemingly more extreme regularity issue than those induced by nonconvex domains. While this loss of smoothness would seem to preclude the use of  $H^1(\Omega)$ -conforming elements, we recall that each unknown is sufficiently smooth in any subdomain excluding the upper corners and that the use of an appropriately weighted least squares functional can remove any pollution effect due to the loss of smoothness in the upper corners. Thus, for this problem, we approximate all unknowns using  $H^1(\Omega)$ -conforming P2 elements (piecewise continuous quadratics), and  $\Omega$  is discretized using a uniform triangulation. We seek a solution method that converges robustly to the solution away from the singularities.

We implement Newton's method within a nonlinear iteration, defining  $\mathbf{u}_{old}$  and  $\mathbf{U}_{old}$  as current approximations of  $\mathbf{u}$  and  $\mathbf{U}$ . The nonlinear inertial term is thus replaced according to  $Re\mathbf{U}\mathbf{u} \rightarrow Re(\mathbf{U}_{old}\mathbf{u} + \mathbf{U}\mathbf{u}_{old} - \mathbf{U}_{old}\mathbf{u}_{old})$ . When the initial approximations are taken as  $\mathbf{U}_{old} = \mathbf{0}$  and  $\mathbf{u}_{old} = \mathbf{0}$ , the first Newton step corresponds to a Stokes solve. Since the computation of the weight function is essentially free relative to the PDE solve, we choose to compute a new weight function during each subsequent Newton step according to algorithm 1. We find that for  $Re = 100$  using a fixed number ( $n = 5$ ) of Newton steps is sufficient to resolve the nonlinearity.

The procedure for each nonlinear step is to minimize the weighted functional

$$\begin{aligned} \mathcal{F}_w(\mathbf{u}, \mathbf{U}, p; \mathbf{u}_{old}, \mathbf{U}_{old}) &= \|w(-\nabla \cdot \mathbf{U} + Re(\mathbf{U}_{old}\mathbf{u} + \mathbf{U}\mathbf{u}_{old} - \mathbf{U}_{old}\mathbf{u}_{old}) + \nabla p)\|^2 \\ &\quad + \|w(\mathbf{U} - \nabla\mathbf{u})\|^2 + \|w\nabla \cdot \mathbf{u}\|^2 + \|w\nabla \times \mathbf{U}\|^2 + \|w\nabla(\text{tr}(\mathbf{U}))\|^2, \end{aligned}$$

where the weight function is computed according to algorithm 1 and (3.4) with element-wise gradient values

$$\mathcal{G}(\tau) = (\|\nabla\mathbf{u}\|_\tau^2 + \|\nabla\mathbf{U}\|_\tau^2 + \|\nabla p\|_\tau^2)^{1/2}.$$

We first show convergence in the following unweighted residual norm on a subdomain that excludes the singularities:  $\Omega_1 = \{(x, y) \in \Omega : y \leq 0.75\}$  and

$$\begin{aligned} \mathcal{R}^{1/2} &= (\|-\nabla \cdot \mathbf{U} + Re\mathbf{U}\mathbf{u} + \nabla p\|_{\Omega_1}^2 + \|\mathbf{U} - \nabla\mathbf{u}\|_{\Omega_1}^2 \\ &\quad + \|\nabla \cdot \mathbf{u}\|_{\Omega_1}^2 + \|\nabla \times \mathbf{U}\|_{\Omega_1}^2 + \|\nabla(\text{tr}(\mathbf{U}))\|_{\Omega_1}^2)^{1/2}. \end{aligned}$$

Figure 4.8 shows convergence of  $\mathcal{R}^{1/2}$  versus the size of each element. For Stokes flow, the adaptively weighted and standard least squares approaches are comparable, but for Navier-Stokes flow at  $Re = 100$ , the adaptively weighted approach shows improved error reduction at all resolutions and a nearly optimal  $\mathcal{O}(h^2)$  rate.

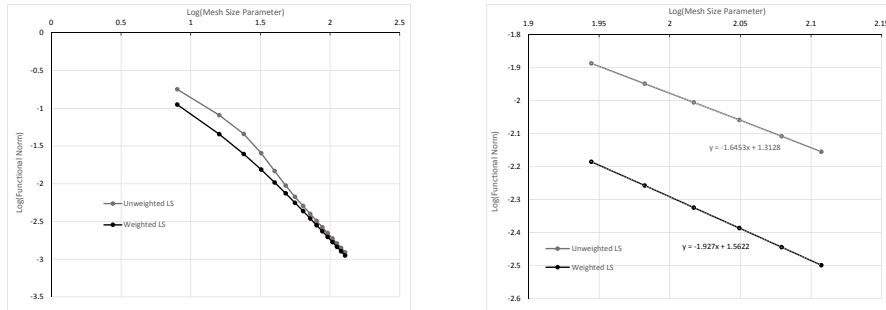


FIG. 4.8. Unweighted residual norm,  $\mathcal{R}^{1/2}$ , versus mesh size parameter,  $h$ , for Stokes flow ( $Re = 0$ , left) and Navier-Stokes ( $Re = 100$ , right).

To further confirm that the adaptively weighted method converges to the exact solution we compare results with benchmark solutions for Stokes flow in [7] and for Navier-Stokes flow in [18].

Figure 4.9 shows plots of the maximum value of the streamfunction (left) and the value of the vorticity at  $(0, 0.95)$  at increasing resolution (see [7] for description of these physical quantities). As the mesh is refined we see that the adaptively weighted approach and standard approaches both reproduce the benchmark values asymptotically.

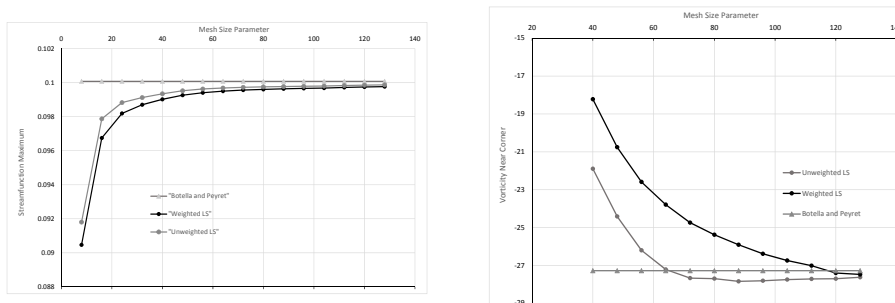


FIG. 4.9. Streamfunction extrema over various mesh sizes (left) and Vorticity values near corner (right).

Figure 4.10 shows components of the velocity along vertical and horizontal lines respectively through the center of the domain, compared with benchmark solution for  $Re = 100$  in [18]. The adaptively weighted approach seems to reproduce the benchmark solution well, even though the problem has severe regularity issues from a discontinuous boundary condition.

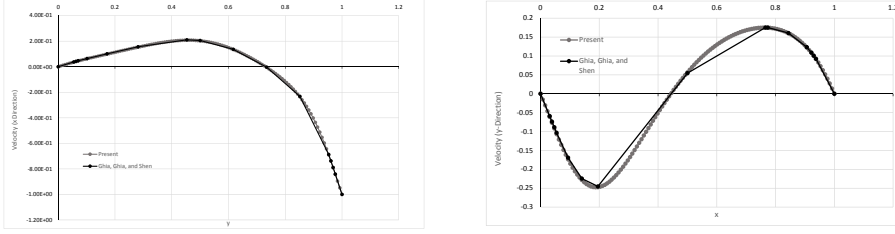


FIG. 4.10. Horizontal (left) and vertical (right) velocity profiles through a horizontal center line for Navier-Stokes flow at  $Re = 100$  compared with a benchmark solution.

**4.5. Example 5: Navier-Stokes, Flow Over a Square Obstacle.** In this section, we analyze the steady state flow around a square obstacle using a stress, velocity, pressure formulation of the Navier-Stokes' Equations:

$$\begin{cases} \nabla \cdot \boldsymbol{\sigma} - \rho \mathbf{u} \cdot \nabla \mathbf{u} = \mathbf{0}, \\ \boldsymbol{\sigma} = \mu(\nabla \mathbf{u} + \nabla \mathbf{u}^T) - pI, \\ \nabla \cdot \mathbf{u} = 0, \end{cases} \quad (4.8)$$

where  $\boldsymbol{\sigma} = \begin{pmatrix} \sigma_{11} & \sigma_{12} \\ \sigma_{21} & \sigma_{22} \end{pmatrix}$  is the total stress tensor,  $\rho$  is the density,  $\mathbf{u} = (u_1, u_2)$  is the velocity,  $\mu = 1$  is the kinematic viscosity,  $p$  is the pressure, and  $I$  is the  $2 \times 2$  identity tensor. We define the Reynolds number to be  $Re = \rho v d / \mu$  where  $v = 1$  is the characteristic velocity and  $d = 1$  is the characteristic length. Thus,  $\rho$  is chosen to correspond to the Reynolds number.

Figure 4.11 shows the domain and boundary conditions used for this test. The full domain is 200 units long and 100 units high with a  $1 \times 1$  square located in the center. Because the solution is symmetric across  $y = 0$ , a half domain is used for computation. The North and West edges of the domain have boundary conditions of  $u_1 = 1$  and  $u_2 = 0$ . No slip boundary conditions are employed on the inner square. The symmetry line along the South edge has boundary conditions setting the  $y$  derivatives of  $u_1$  and  $p$  to be zero. The shear stresses,  $\sigma_{12}$  and  $\sigma_{21}$ , along with  $u_2$  are also set to zero along the South edge. The East edge is set to be consistent with a fully developed constant flow. It employs a zero normal velocity gradient and zero pressure which implies each component of  $\boldsymbol{\sigma}$  to be zero as well.

Letting  $\mathbf{u}_{old}$  represent a current approximation (initially starting with  $\mathbf{u}_{old} = \mathbf{0}$ ), the linearized, weighted least squares functional is given by

$$\begin{aligned} \mathcal{F}_w(\boldsymbol{\sigma}, \mathbf{u}, p; \mathbf{u}_{old}) = & \|w(\nabla \cdot \boldsymbol{\sigma} - \rho(\mathbf{u}_{old} \cdot \nabla \mathbf{u} + \mathbf{u} \cdot \nabla \mathbf{u}_{old} - \mathbf{u}_{old} \cdot \nabla \mathbf{u}_{old}))\|^2 \\ & + \|w(\boldsymbol{\sigma} - (\nabla \mathbf{u} + \nabla \mathbf{u}^T) + pI)\|^2 + \|w(\nabla \cdot \mathbf{u})\|^2. \end{aligned} \quad (4.9)$$

For the adaptively weighted method,  $w$  is chosen from a previous approximation according to element-wise gradient values,

$$\mathcal{G}(\tau) = \frac{1}{h_\tau^2} (\|\nabla \boldsymbol{\sigma}^h\|_\tau^2 + \|\nabla \mathbf{u}^h\|_\tau^2 + \|\nabla p^h\|_\tau^2)^{1/2} \quad (4.10)$$

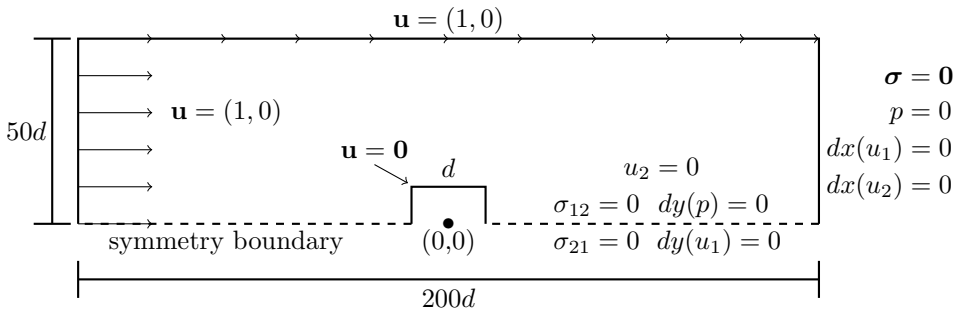


FIG. 4.11. Domain and boundary conditions for Stokes flow example.

and (3.3) for the weight. For comparison, we also define an *a priori* weighting approach, which uses a predefined weight function with  $w \sim r^\beta$  (Figure 4.12) near each reentrant corner and  $w = 1$  away from the neighborhood of each corner. Based on the known regularity of (4.8) we may use  $\beta = 1.5$  to accelerate convergence. For the standard approach,  $w = 1$  over the entire domain. Figure 4.12 shows a comparison of one adaptively generated weight function and the *a priori* weight function used.



FIG. 4.12. Weight functions on reentrant corners for the adaptive weight (left) and *a priori* weight (right). White regions represent  $w = 1$  while darker regions are closer to  $w = 0$ .

The computational domain is discretized into  $N$  total elements, where we define  $n$  as the number of elements on each side of the square obstacle. Figure 4.13 shows a representative mesh (with  $n = 10$ ) over the computational domain and a detail of the local mesh around the square. Numerical results in figures 4.15 and 4.16 use  $n = 30$ . Computational meshes M1-M4 use  $n = 4, 8, 16,$  and  $32$  respectively.

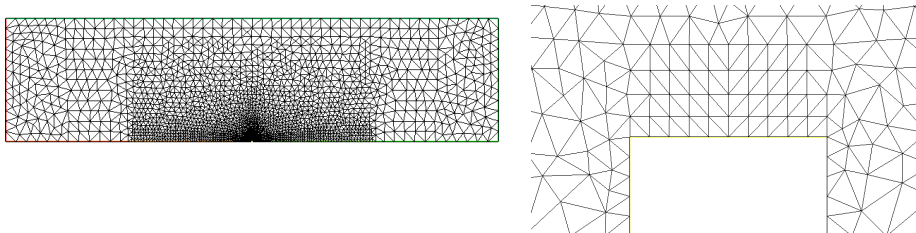


FIG. 4.13. Low resolution mesh ( $n = 10$ ) over the computational domain (left) and a detail around the obstacle (right).

We choose the FE spaces based upon the structure of the equations in the system, with  $\boldsymbol{\sigma}^h \in RT_1$  (the next to lowest space of  $H(\text{div})$  conforming Raviart Thomas elements),  $\mathbf{u}^h \in P_2$  (continuous piecewise quadratic elements), and  $p^h \in P_{1dc}$  (discontinuous piecewise linear elements).

Table 4.4 summarizes convergence in the functional norm for the three approaches: standard ( $w = 1$ ), adaptive, and *a priori*. We define a composite global mesh size parameter  $h = N^{-1/2}$  where  $N$  is the number of elements in the domain. We estimate the rate of convergence to be  $O(h^r)$ , with the weighted functional norm  $\mathcal{F}_w^{1/2} = (\mathcal{F}_w(\boldsymbol{\sigma}^h, \mathbf{u}^h, p^h))^{1/2}$ , where  $r = \log(\mathcal{F}_{w_1}^{1/2}/\mathcal{F}_{w_2}^{1/2})/\log(h_1/h_2)$ .

Convergence is slow for the standard approach while each of the weighted approaches has better convergence.

Mesh	$N$	$\mathcal{F}^{1/2}$ standard	$\mathcal{F}_w^{1/2}$ adaptive	$\mathcal{F}_w^{1/2}$ <i>a priori</i>
M1	720	0.5682	0.4647	0.5246
M2	2880	0.3915	0.2422	0.3117
M3	11520	0.2873	0.1211	0.1253
M4	46080	0.2196	0.0680	0.0493
rate $\approx$		0.39	0.83	1.35

TABLE 4.4

Functional Norm convergence comparison (at  $Re = 20$ ) between the standard least squares approximation ( $w = 1$ ), the adaptively weighted approach, and the *a priori* weighted approach. The meshes are generated in a nested refinement pattern with the structure shown in Figure 4.13. Convergence rate is estimated from data on the two finest mesh levels.

To further examine computational results, we measure the size of the downstream recirculation eddy and the drag coefficient for a range of Reynolds numbers., comparing values to benchmark solutions published in [31] (noted below as Sen).

We define the reattachment length to be the horizontal distance from the downstream edge of the square to the transition point between recirculation and flow as shown in Figure 4.14. Computational results summarized in Figure 4.15 show that both weighted approaches match the values in the reference solution well, while the standard approach significantly under predicts the size of the downstream vortex size.

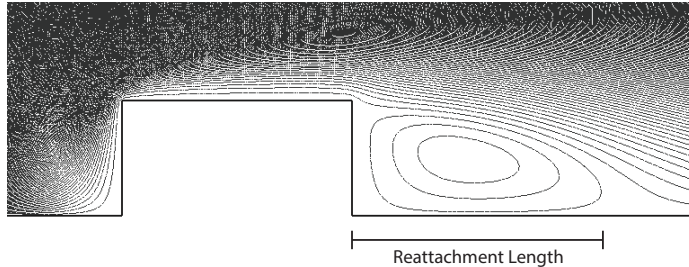


FIG. 4.14. The reattachment length is measured as the distance from the back edge of the square to the transition point between recirculation and flow.

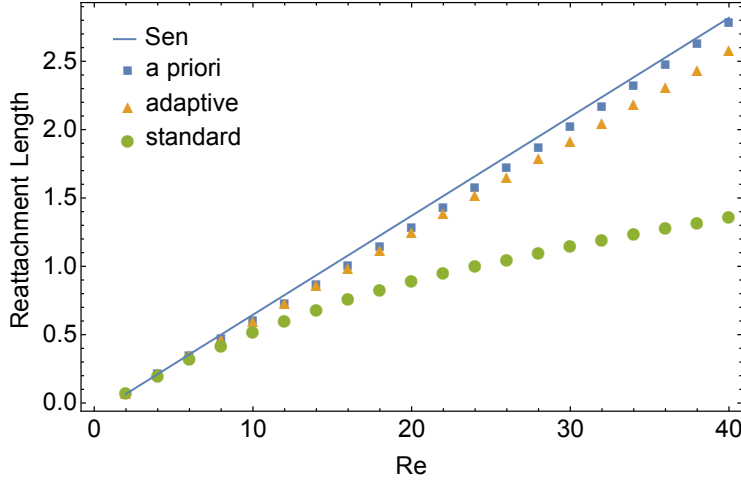


FIG. 4.15. Comparison of reattachment length between different weighting methods (on  $n = 30$ ) and the previous work of Sen, et al. At very low Reynolds numbers all methods can be used to good approximation. At  $Re > 10$  only the a priori and adaptive weighting methods continue to be a good approximations. At relatively low mesh resolution, the a priori and adaptive weighting methods produce significantly better results than the standard method.

We define the general coefficient of drag to be

$$C_D = \frac{2}{Re} \int_s (\boldsymbol{\sigma} \hat{n} \cdot \hat{i}) ds \quad (4.11)$$

where  $\hat{n}$  is a unit vector normal to the surface of the obstacle, and  $\hat{i}$  is a unit vector in the horizontal direction [33]. We can decompose the general formula to this specific setup, relative to the full domain, as

$$C_D = C_{Dp} + C_{Dv} \quad (4.12)$$

where

$$C_{Dp} = \frac{2}{Re} F_p = \frac{2}{Re} \int_{E,W} p dy \quad (4.13)$$

is the pressure drag, where  $F_p$  is the force due to pressure,

$$C_{Dv} = \frac{2}{Re} F_v = \frac{2}{Re} \int_{N,S} \partial_y u_1 dx \quad (4.14)$$

is the viscous drag, where  $F_v$  is the force due to viscous shear. Here,  $N, S, E, W$  represents the North, South, East, and West sides of the square obstacle respectively. Figure 4.16 compares drag coefficient values for a range of Reynolds numbers for the three approaches, each computed on a mesh with  $n = 30$ . As before, the standard approach under predicts the values while each of the weighted methods produce values close to the reference solution. As a final consideration, we report convergence of drag coefficients and reattachment lengths for a fixed Reynolds number ( $Re = 20$ ) on a sequence of mesh refinements. For each method, values seem to be approaching that of the reference solution, but the weighted methods show better convergence to the reference values, indicating a mitigation of the pollution effect induced by the nonsmooth solution at the reentrant corners.

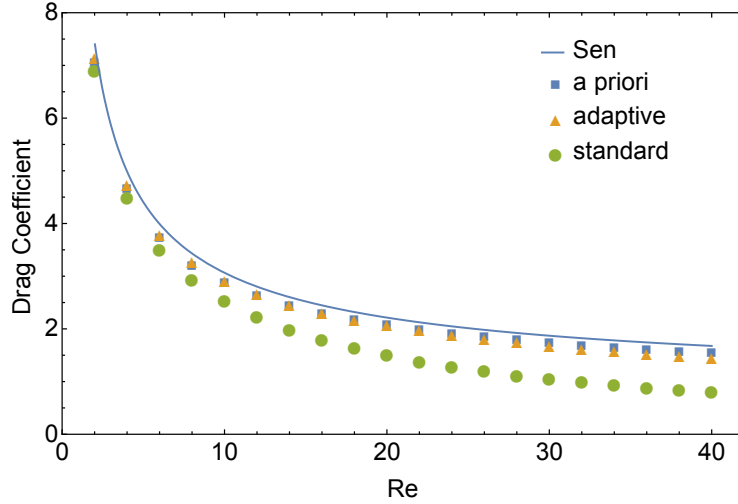


FIG. 4.16. Comparison of the drag coefficient between different weighting methods (on  $n = 30$ ) and the previous work of Sen et al. [31]. Although on a comparatively coarse mesh, both the a priori and adaptive weighting methods are a good approximation to the reference solution.

Mesh	$C_D$ standard	$C_D$ adaptive	$C_D$ a priori	RL standard	RL adaptive	RL a priori
M1	0.60	0.92	0.74	—	—	—
M2	0.87	1.43	1.21	0.41	0.86	0.71
M3	1.14	1.78	1.86	0.64	1.15	1.20
M4	1.46	2.04	2.09	0.86	1.26	1.29

TABLE 4.5

Drag coefficient and reattachment length convergence comparison (at  $Re = 20$ ) between the standard least squares approximation ( $w = 1$ ), the adaptively weighted approach, and the a priori weighted approach. The published values for the coefficient of drag and reattachment length are  $C_d \approx 2.21$  and  $RL \approx 1.37$ , [31].

**5. Conclusion.** The adaptively weighted least squares approach presented here represents a practical way to treat problems with nonsmooth solutions without requiring the use of exotic finite element spaces or special reformulations of the problem. The general idea can be implemented naturally within an adaptive mesh refinement routine, or within a nonlinear or implicit time stepping iteration, and the additional cost of generating the weight function is small compared with the work required for the full PDE solve. Numerical results demonstrate that the pollution effect due to problems with nonsmooth solutions can be reduced or eliminated, suggesting that the adaptively weighted approach is able to minimize the error in a more optimal norm than using standard  $L^2$  minimization principles.

REFERENCES

[1] TH. Apel and B. Heinrich. Mesh refinement and windowing near edges for some elliptic problem. *SIAM J. Numer. Anal.*, 31(3):695–708, 1994.  
 [2] M. Berndt. *Adaptive Refinement and the treatment of discontinuous coefficients for multilevel first-order system least squares (FOSLS)*. PhD thesis, University of Colorado, Boulder,

- 1999.
- [3] M. Berndt, T.A. Manteuffel, S.F. McCormick, and G. Starke. Analysis of first-order system least squares (FOSLS) for elliptic problems with discontinuous coefficients: part I. *SIAM J. Numer. Anal.*, 43(1):386–408, 2005.
  - [4] M. Berndt, T.A. Manteuffel, S.F. McCormick, and G. Starke. Analysis of first-order system least squares (FOSLS) for elliptic problems with discontinuous coefficients: part II. *SIAM J. Numer. Anal.*, 43(1):409–436, 2005.
  - [5] S. Bidwell, M. Hassell, and C.R. Westphal. A weighted least squares finite element method for elliptic problems with degenerate and singular coefficients. *Math. Comp.*, 82:672–688, 2013.
  - [6] D. Boffi, F. Brezzi, L.F. Demkowicz, R.G. Duran, R.S. Falk, and M. Fortin. *Mixed Finite Elements, Compatibility Conditions, and Applications*, volume 1939 of *Lecture Notes in Mathematics*. Springer-Verlag, 2008. Edited by D. Boffi and L. Gastaldi.
  - [7] O. Botella and R. Peyret. High-Re solutions for incompressible flow using the Navier-Stokes equations and a multigrid method. *J. Computational Physics*, 48:387–411, 1982.
  - [8] J. Bramble, R. Lazarov, and J. Pasciak. A least-squares approach based on a discrete minus one inner product for first order systems. *Math. Comp.*, 66(219):935–955, 1997.
  - [9] F. Brezzi and M. Fortin. *Mixed and Hybrid Finite Element Methods*. Springer-Verlag, 1991.
  - [10] P. Burda. On the fem for the Navier-Stokes equations in the domains with corner singularities. In M. Křížek, P. Neittaanmäki, and R. Stenberg, editors, *Finite Element Methods*, pages 41–52. Marcel Dekker, Inc., New York, NY, USA, 1998.
  - [11] P. Burda, J. Novotny, and J. Sistek. Accurate solution of corner singularities in axisymmetric and plane flows using adjusted mesh of finite elements. In Clinton Groth and David W. Zingg, editors, *Computational Fluid Dynamics 2004*, pages 463–468. Springer Berlin Heidelberg, 2006.
  - [12] Z. Cai, T.A. Manteuffel, and S.F. McCormick. First-order system least squares for the Stokes equations, with application to linear elasticity. *SIAM J. Numer. Anal.*, 34(5):1727–1741, 1997.
  - [13] Z. Cai, T.A. Manteuffel, S.F. McCormick, and J. Ruge. First-order system  $\mathcal{LL}^*$  (FOSLL\*): Scalar elliptic partial differential equations. *SIAM J. Numer. Anal.*, 39(4):1418–1445, 2002.
  - [14] Z. Cai and C.R. Westphal. A weighted H(div) least-squares method for second-order elliptic problems. *SIAM J. Numer. Anal.*, 46(3):1640–1651, 2008.
  - [15] Z. Cai and C.R. Westphal. An adaptive mixed least-squares finite element method for viscoelastic fluids of Oldroyd type. *J. Non-Newton. Fluid. Mech.*, 159:72–80, 2009.
  - [16] G. F. Carey and H. T. Dinh. Grading functions and mesh redistribution. *SIAM J. Numer. Anal.*, 22(5), 1985.
  - [17] L. Demkowicz and J. Gopalakrishnan. Analysis of the DPG method for the Poisson equation. *SIAM J. Numer. Anal.*, 49:1788–1809, 2011.
  - [18] U. Ghia, K. N. Ghia, and C. T. Shin. Benchmark spectral results on the lid-driven cavity flow. *Computers & Fluids*, 27(4):421433, 1998.
  - [19] P. Grisvard. *Elliptic Problems in Nonsmooth Domains*. Pitman, 1985.
  - [20] M.D. Gunzburger and P.B. Bochev. *Least-Squares Finite Element Methods*. Springer, 2009.
  - [21] F. Hecht. New development in FreeFem++. *J. Numer. Math.*, 20(3-4):251–265, 2012.
  - [22] S.D. Kim, C-O. Lee, T.A. Manteuffel, S.F. McCormick, and O. Röhrle. First-order system least squares for the Oseen equations. *J. Numer. Lin. Alg. Appl.*, 13:461–486, 2006.
  - [23] V.A. Kondratiev. Boundary problems for elliptic equations in domains with conical or angular points. *Trans. Moscow Math. Soc.*, 16:227–313, 1967.
  - [24] V.A. Kozlov, V.G. Maz'ya, and J. Rossmann. *Elliptic Boundary Value Problems in Domains with Point Singularities*, volume 52. American Mathematical Society, 1997.
  - [25] V.A. Kozlov, V.G. Maz'ya, and J. Rossmann. *Spectral Problems Associated with Corner Singularities of Solutions to Elliptic Equations*, volume 85. American Mathematical Society, 2001.
  - [26] J.R. Kweon. Regularity of solutions for the Navier-Stokes system of incompressible flows on a polygon. *J. Differ. Equations*, 235(1):166–198, 2007.
  - [27] E. Lee, T.A. Manteuffel, and C.R. Westphal. Weighted-norm first-order system least squares (FOSLS) for problems with corner singularities. *SIAM J. Numer. Anal.*, 44(5):1974–1996, 2006.
  - [28] E. Lee, T.A. Manteuffel, and C.R. Westphal. Weighted-norm first-order system least squares (FOSLS) for div/curl systems with three dimensional edge singularities. *SIAM J. Numer. Anal.*, 46(3):1619–1639, 2008.
  - [29] K. Liu, T. Manteuffel, S. McCormick, J. Ruge, and L. Tang. Hybrid first-order system least squares (hybrid-FOSLS) finite element methods with application to Stokes equations.

- SIAM J. Numer. Anal.*, 51:2214–2237, 2013.
- [30] R. Nochetto, K. Siebert, and A. Veerer. Theory of adaptive finite element methods: An introduction. In Ronald DeVore and Angela Kunoth, editors, *Multiscale, Nonlinear and Adaptive Approximation*, pages 409–542. Springer Berlin Heidelberg, 2009.
  - [31] S. Sen, S. Mittal, and G. Biswas. Flow past a square cylinder at low Reynolds numbers. *Int. J. Numer. Meth. Fluids*, 67:1160–1174, 2011.
  - [32] J.A. Sethian and J. Wilkening. A numerical model of stress driven grain boundary diffusion. *J. Comput. Phys.*, 193(1):275–305, 2004.
  - [33] A. Sharma and V. Eswaran. Heat and fluid flow across a square cylinder in the two-dimensional laminar flow regime. *Taylor & Francis Online*, 45:247–269, 2004.
  - [34] Y. Sun and C.R. Westphal. An adaptively weighted Galerkin finite element method for boundary value problems. *CAMCoS*, 10(1):27–41, 2015.
  - [35] J. Wilkening. *Mathematical Analysis and Numerical Simulation of Electromigration*. PhD thesis, University of California, Berkeley, 2002.